Journal of
Ceramic Science
and Technology

J. Ceram. Sci. Tech., 07 [03] 263-276 (2016)
DOI: 10.4416/JCST2016-00011
available online at: http://www.ceramic-science.com

Biocompatibility of Hydroxyapatite-Alumina and Hydroxyapatite-Zirconia Composites including Commercial Inert Glass (CIG) as a Ternary Component

B. Bulut*[1], Z.E. Erkmen[2], E.S. Kayali[1]

[1]Metallurgical and Materials Engineering Dept., Faculty of Chemical and Metallurgical Engineering, Istanbul Technical University, Istanbul, Turkey
[2]Metallurgical and Materials Engineering Dept., Faculty of Engineering, Marmara University, Istanbul, Turkey

received February 1, 2016; received in revised form April 19, 2016; accepted May 27, 2016

Abstract

Hydroxyapatite (HA), chemical formula $Ca_{10}(PO_4)_6(OH)_2$, is a very popular bioceramic for orthopedic and dental applications. Although HA has excellent biocompatibility, its inferior mechanical properties make it unsuitable for load-bearing implant applications. Therefore, HA should be strengthened by a secondary phase to produce a composite that possesses robust mechanical properties. The aim of this study was to compare the microstructural and mechanical properties and biocompatibility of HA-Al_2O_3 and HA-ZrO_2 composites with the addition of 5 and 10 wt% commercial inert glass (CIG) independently and to determine from the studied composites the one with the most suitable composition for biomedical applications. The powders were pressed and then, the pellets were sintered between 1000 – 1300 °C for four hours. The thermodynamic analyses of the samples were performed by means of DTA followed by the thermodynamic analysis program FactSage. Microstructural characterizations were carried out using SEM + EDS and XRD, while hardness and compression tests were performed to measure the mechanical properties. The results showed that the compressive strength and the microhardness of HA-Al_2O_3 composites increased with rising CIG content and increasing sintering temperature. On the other hand, for HA-ZrO_2 composites, increasing CIG content caused an elevation in hardness and a decrease in compressive strength values at 1300 °C. The biocompatibility tests (*in vitro* and *in vivo*) were performed on those composites that possessed the highest physical and mechanical properties. In conclusion, the optimum CIG content was determined to improve the mechanical properties and biocompatibility of the composites. The mechanical properties and biocompatibility of HA-Al_2O_3 composites have been found to be lower than those of HA-ZrO_2 composites. In this study, the ideal composite was selected as HA-ZrO_2- 5 wt% (HZC5) sintered at 1200 °C.

Keywords: Hydroxyapatite, ceramics, composites, microstructure, mechanical properties, biocompatibility

I. Introduction

Calcium phosphate (CaP) ceramics are widely used to repair and reconstruct damaged parts of the human skeleton [1,2]. Different types of CaP, such as hydroxyapatite (HA), tetra calcium phosphate (TTCP), tricalcium phosphate (TCP), dicalcium phosphate anhydrous (DCP), amorphous calcium phosphate (ACP) and biphasic calcium phosphate (BCP), are available for use as hard tissue substitutes [3]. Hydroxyapatite (HA) ($Ca_{10}(PO_4)_6(OH)_2$) is the most promising material for bone replacement based on its chemical composition. It is similar to the mineral parts of bone and tooth and confers excellent biocompatibility and osteoconductivity properties [4,5]. Additionally, HA materials do not exhibit any cytotoxic effects [6]. However, the application of HA is limited for use as implant material because of its inferior mechanical properties [7,8]. There have been many investigations aimed at improving the mechanical properties of HA, like preparing them as composite materials [9]. Addition of second-phase ceramic materials (e.g. zirconia, titania or alumina) into the HA matrix for enhancing strength and toughness has been an interesting subject in recent years [10]. Among them, alumina (Al_2O_3) has been widely recognized as a reinforcing agent based on its excellent wear resistance, high hardness and high abrasion resistance [11,12]. The Al_2O_3 ceramic used in biomedical applications is α-Al_2O_3, known as corundum [13].

Zirconia (ZrO_2) is also a well-known reinforcing agent as a result of its relatively high mechanical strength, toughness, wear resistance, corrosion resistance and biocompatibility [14,15]. At ambient pressure, ZrO_2 polymorphs occur in three forms; monoclinic (M), tetragonal (T), and cubic (C) depending on the temperature [15,16]. As a result of phase transformation, pure and single-phase ZrO_2 tends to fracture even at room temperature, leading to deterioration in mechanical properties and consequently making

* Corresponding author: berrakbulut@hotmail.com

it unsuitable for clinical applications. Therefore, ZrO_2-based composites possess enhanced toughness following controlled phase transformation of stabilized ZrO_2 doped with yttria (Y_2O_3) (Y-TZP) [16]. Bioactive glasses and glass ceramics are biomaterials with osteoconductive and osteoproductive properties as well as being able to repair and replace diseased or damaged bone [8, 17]. The glass ceramics after sintering have superior mechanical properties, enhanced biocompatibility, bioactivity, and no toxicity, making them useful as a biomaterial in artificial bone and dental implants [18]. These properties result from their progressive dissolution in physiological medium, where the release of calcium, phosphate, and sodium ions will undergo formation of an apatite layer that in turn creates a strong bond with the surrounding bone tissues [17, 19].

There are a number of studies that have investigated HA-Al_2O_3, HA-ZrO_2 and HA-CIG composites. Yelten *et al.* [20] looked at HA-Al_2O_3 biocomposite powders. In this study, Al_2O_3 was derived with the sol-gel method, then, mixed with HA powders. The gel mixture was heat-treated at 1300 °C for two hours. XRD results showed that the powders were composed of α-alumina and apatite-based phases, such as tricalcium phosphate and HA, forming a highly porous structure observed by SEM. Pujiyanto *et al.* [21] studied a porous HA-ZrO_2 composite in which HA was synthesized from local gypsum by means of the microwave hydrothermal method. Different amounts of ZrO_2 (0, 20, 30 and 40 wt%) were mixed with HA for six hours and green pellets obtained after pressing were then sintered at 1450 °C for two hours. It was then determined that the compressive strength of the porous HA-ZrO_2 composite decreased when the ZrO_2 percentage increased up to 40 wt%. This might be a consequence of enhanced porosity, cracked ZrO_2 grain, reaction of ZrO_2 with HA producing $CaZrO_3$, β-TCP and α-TCP and cracking of the HA matrix because of the phase change of tetragonal ZrO_2 into monoclinic ZrO_2. Salman *et al.* [22] investigated the sintering effect on the mechanical properties of composites made of bovine hydroxyapatite (BHA) and commercial inert glass (CIG). In this study, HA was derived from calcined bovine and was doped with 5 and 10 wt% CIG. Composite materials were then obtained by sintering. Addition of glass components into the HA structure in small quantities is very popular for improving sinterability and thus improving the mechanical performance of HA biomaterials. The experimental results showed that an optimum amount of glass was sufficient for obtaining promising compression strength and microhardness values, indicating suitability for load-bearing biomedical applications.

The objective of this study was to compare the microstructural and mechanical properties and biocompatibility of HA-Al_2O_3 and HA-ZrO_2 composites with the addition of 5 and 10 wt% commercial inert glass (CIG), separately.

II. Materials and Methods

(1) Materials

Commercial synthetic hydroxyapatite (Acros Org., BE) was used as the major component. Alumina (α-corundum) (Seranit Org, TR), zirconia (doped with 10 – 15 % Y_2O_3) (Alfa Aesar, DE) and commercial inert glass (CIG) were selected as additives. Table 1 shows the chemical analysis of the CIG obtained from conventional window glass [23]. Firstly, the 90 wt% HA-10 wt% Al_2O_3 and the 90 wt% HA-10 wt% ZrO_2 powders were mixed separately for 24 h in a ball mill, after which the powders were remixed and ball-milled with 5 and 10 wt% CIG for 4 h. In this way, HA-Al_2O_3-5 wt% CIG (HAC5), HA-Al_2O_3-10 wt% CIG (HAC10) and HA-ZrO_2-5 wt% CIG (HZC5), HA-ZrO_2-10 wt% CIG (HZC10) composites were produced. The powders were pressed at 350 MPa to form cylindrical pellets (height: 11 mm; diameter: 11 mm) and then they were sintered at 1000, 1100, 1200, and 1300 °C for 4 h (+ 5 °C min^{-1}).

Table 1: Chemical analysis of the CIG.

Oxide	wt%
SiO_2	68.80
Na_2O	17.02
CaO	9.25
MgO	1.77
Fe_2O_3	0.084
TiO_2	0.017
Al_2O_3	2.15
Cr_2O_3	0.012
CuO	0.0036
Other	Trace Amount

(2) Characterization techniques and mechanical tests

Density, Vickers microhardness, and compression strength tests were performed to determine the mechanical properties of the composites. The density of the samples was gauged with the Archimedes method. The hardness of the samples was measured with a Vickers microhardness testing system (HMV Shimadzu, JP), using 200 g load for 15 s and the compression tests were carried out using a Universal Testing machine (Shimadzu, JP) at a crosshead speed of 3 mm/min (sample diameter: 11 mm; sample height 11 mm). The powders were analyzed with Differential Thermal Analysis (DTA) (TA Instruments SDT Q600, US) up to 1300 °C using the 10 °C/min heating rate in an air atmosphere. The thermodynamic analysis software FactSage [24] was used to determine stable phases and their physical state between transformation temperatures. x-ray diffraction (XRD) analysis was carried out using a Brucker D8-Advanced X-ray diffractometer (DE) with Cu Kα radiation. Scanning Electron Microscopy (SEM) (Jeol JSM-5910 LV – Low Vacuum Scanning, US) and Energy Dispersive Spectroscopy (EDS) (Oxford Inca Energy 200, UK) were used for microstructural characterization of the composites.

(3) Biocompatibility Tests

In order to investigate the biocompatibility behavior of the samples and whether they had robust mechanical properties, *in vitro* and *in vivo* tests were performed. *In vitro* tests were carried out in simulated body fluid (SBF), prepared according to the Kokubo prescription [25,26]; under controlled temperature (36.5 °C) and pH (7.4). Samples were removed from the solution after 1, 2, 3, and 4 weeks. The morphology of the intensive apatite layer on the surface and microstructure of the samples were examined with SEM. After *in vitro* and *in vivo* tests had been performed, the HZC5 composite sintered at 1200 °C showed the best performance.

For the case of *in vivo* tests, the cells were prepared according to the method of Maniatopoulos *et al.* [27]. Rat bone marrow stem cells were isolated from the femora of 5-week-old male Wistar rats and cultured in 75-cm^2 flasks in α-MEM (Sigma Aldrich, Tokyo, Japan) with 10 % fetal bovine serum (Invitrogen, Tokyo, Japan) at 37 °C in a humidified atmosphere consisting of 95 % air and 5 % CO_2. After 24 hours, fresh medium was replaced and the cells were allowed to grow until 80 % confluency. The media were replaced every two days. Cells were expanded *in vitro* until passage three and once confluent, the culture medium was aspirated and the flask was washed with sterile phosphate buffer saline (PBS). the cells being detached using 10 % Trypsin-EDTA (Invitrogen, Tokyo, Japan). The cells were centrifuged at 2000 rpm for 5 minutes and $1x10^4$ cells were seeded into each well in a 24-well plate in the absence of the experimental materials. The cells were next allowed to adhere and spread for three days before the culture medium was replaced with osteogenic medium (50 μg/ml ascorbic acid, 10 mM β-glycerophosphate, 10 nM dexamethasone). The experimental groups were: control group (empty, tissue culture plate) and the HZC5 composite group sintered at 1200 °C. The samples were placed in each respective well on top of the cells. Cell culture on the plastic surface was used as a control. The culture media were exchanged every two days until the end of the experiment.

Growth and viability of MSCs: Cell proliferation and viability was assessed using AlamarBlue™ stain (Invitrogen, Tokyo, Japan) in accordance with the manufacturer's protocol. After 7, 10, and 14 days in incubation, 100 μL of AlamarBlue™ was added into each culture well and incubated for three hours at 37 °C in a humidified atmosphere (95 % air and 5 % CO_2). The absorbance was read at l = 570 nm in a multi-plate reader (Corona Electric MTP-650, Tokyo, Japan). A separate set of cells was used for plotting a calibration curve based on cell number versus absorbance intensity at each time-point.

Quantification of alkaline phosphatase (ALP) activity: At 7, 10, and 14 days after culturing in an osteogenic medium, the cells were washed thrice with PBS, scraped and lysed by 0.1 % Triton X100 (Sigma Aldrich, Tokyo, Japan). The extracts were assayed based on an ALP detection kit (Wako Chemical Co. Ltd., Tokyo, Japan) for ALP activity. They were reacted with *p*-nitrophenyl phosphate solution, prepared according to the manufacturer's instructions, and their absorbance was detected at l = 405 nm in a multi-plate reader (Corona Electric MTP-650, Tokyo, Japan). A separate calibration plot was made for each time-point. ALP activities were normalized against total protein content from each extract. The levels of activity were standardized with the amount of protein in the cell lysate solution (units/μg of protein). Total protein was determined with a QuantiPro BCA Assay Kit (Sigma Aldrich, Tokyo, Japan) based on the principle of the bicinchoninic acid (BCA) assay. Cell lysis was reacted with BCA solution prepared according to the manufacturer instructions and incubated at 37 °C. After two hours, the absorbance was read at 562 nm using the same multi-plate reader.

Calcium mineralization assay by Alizarin Red S: At 7, 10, and 14 days of culture in osteogenic medium, the cells were washed with PBS thrice and fixed with 10 % formaldehyde (Wako Chemical Co. Ltd., Tokyo, Japan) for 15 min at room temperature. The cells were then stained with Alizarin Red S solution (Sigma Aldrich, Tokyo, Japan) and incubated for 15 min at room temperature with gentle shaking. Following this, the Alizarin solution was aspirated and the cells were washed again thrice before observation under a light microscope. Calcium deposit nodules were observed based on their distinct red color. The quantification of the Alizarin Red S was based on destaining using 10 % cetylpyridinium chloride (CPC) in 10 mM sodium phosphate (Sigma Aldrich, Tokyo, Japan) for 15 min at room temperature. Each extract was diluted 10-fold in 10 % CPC solution; and the Alizarin Red S concentration was determined by means of absorbance measurement at 562 nm on a multi-plate reader as done previously.

Statistical analysis: All data were examined based on five different measurement values and repeated in triplicate. The results are presented as standard deviation. Statistical analysis was based on one-way analysis of variance (ANOVA) with Turkey's post hoc test used for multiple comparisons (SPSS, IBM, USA) where a p-value < 0.05 was considered significant.

III. Results and Discussion

(1) Density results

Fig. 1 depicts the density data and Table 2 summarizes the porosity values of composites sintered at different temperatures.

As seen in Fig. 1, with increasing sintering temperature, the density of the composites increased while their porosity decreased. HAC10 composite has the lowest porosity and the highest density of the HAC composites. HZC5 composite has the lower porosity and the highest density of the HZC composites. When we compare both composites the highest density was obtained in the HZC5 composite sintered at 1300 °C and the lowest porosity was obtained in the HAC10 composite sintered at 1300 °C.

Table 2: The porosity values of composites sintered at different temperature.

	Porosity (%)			
	HAC		HZC	
Temperature (°C)	5 wt% CIG	10 wt% CIG	5 wt% CIG	10 wt% CIG
1000	40.89 ± 1.51	37.96 ± 0.85	35.86 ± 0.66	42.48 ± 0.10
1100	40.03 ± 0.24	37.49 ± 0.83	31.67 ± 1.61	31.81 ± 0.08
1200	35.86 ± 0.66	31.58 ± 1.24	18.29 ± 3.56	22.71 ± 1.67
1300	19.10 ± 2.85	05.49 ± 0.94	08.44 ± 0.42	19.84 ± 0.86

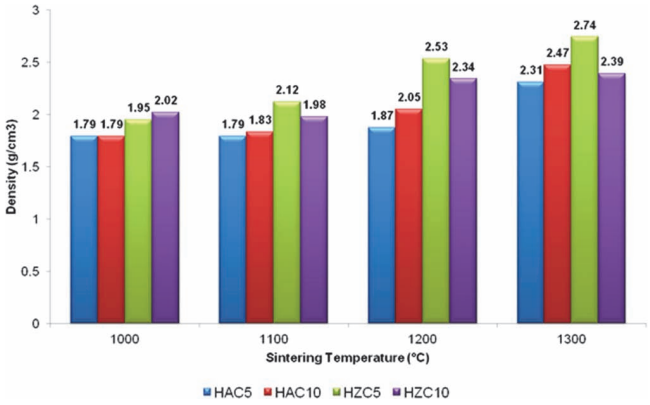

Fig. 1: The density values of composites sintered at different temperatures.

(2) Thermodynamic analysis

Fig. 2 shows the DTA analysis of the HAC5 composites while Fig. 3 illustrates the corresponding Fact Sage thermodynamic equilibrium results in which the transformation of hydroxyapatite is intentionally separated to elucidate it. Similarly, Fig. 4 describes the DTA analysis whereas Fig. 5 portrays the corresponding equilibrium results of the HAC10 composites. It was clearly seen that the thermodynamic computation indicated that while the amount of hydroxyapatite (HA) ($Ca_{10}(OH)_2(PO_4)_6$) phase was decreasing, the whitlockite (W) ($Ca_3(PO_4)_2$) phase started to form at 1100 °C thermodynamically for HA-Al_2O_3 composites.

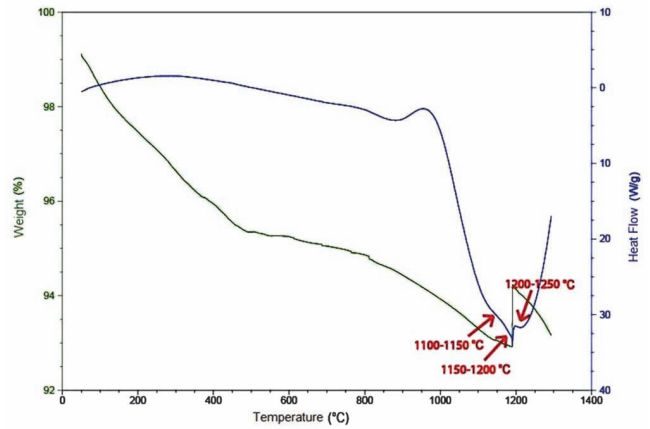

Fig. 2: The DTA analysis result of the HAC5 composites.

With rising temperature, almost all HA present in the structure was transformed to the W. Gehlenite phase ($CaAl_2SiO_7$) and liquid slag formed above 1200 °C. The endothermic peak temperatures were observed at 1100 – 1150 °C, 1150 – 1200 °C and 1200 – 1250 °C for HAC5 corresponding to W and Gehlenite phase formations (Fig. 2). Similar behavior occurred for HAC10 at 1100 – 1200 °C in Fig. 4, confirming with thermodynamic predictions that given in Fig. 3 and Fig. 5. HA transformation to W started nearly at 1125 °C and ended at 1225 °C observed in Fig. 3. The 5 wt% weight change seen in Fig. 2 was the result of water evaporation. Equation 1 represents the transformation of HA.

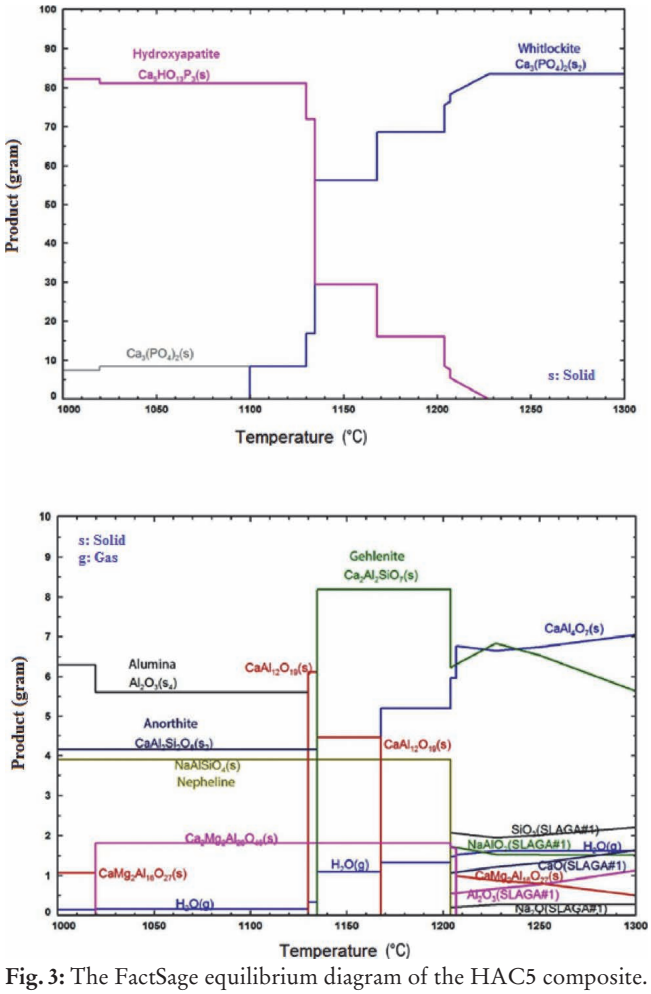

Fig. 3: The FactSage equilibrium diagram of the HAC5 composite.

$$Ca_{10}(OH)_2(PO_4)_6 \rightarrow 3Ca_3(PO_4)_2 + CaO + H_2O \quad (1)$$

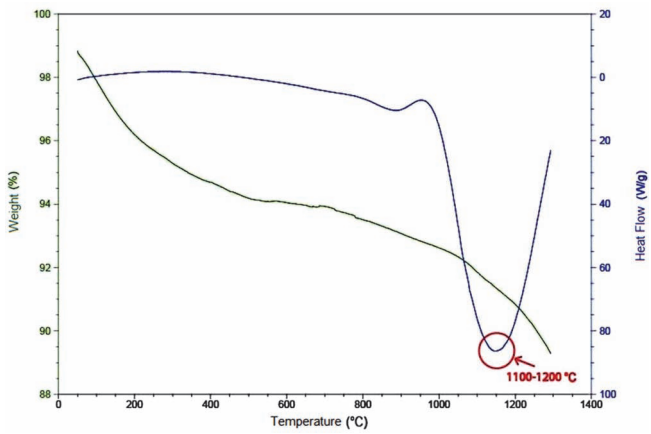

Fig. 4: The DTA analysis result of the HAC10 composite.

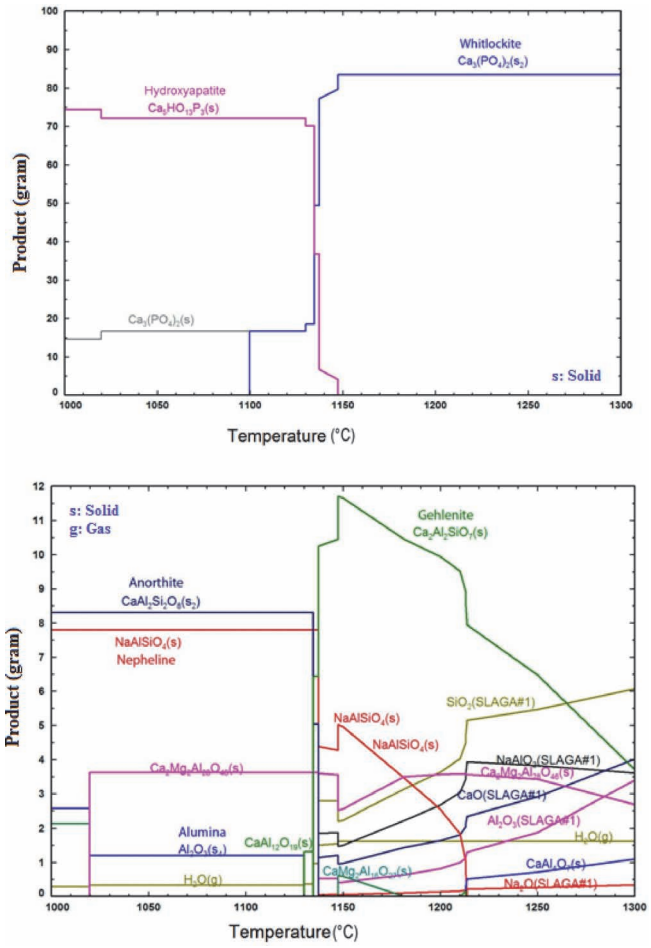

Fig. 5: The FactSage equilibrium diagram of the HAC10 composite.

Fig. 6, Fig. 7 and Fig. 8, Fig. 9 illustrate the equilibrium results and the DTA analysis of the HZC5 and HZC10 composites, respectively. The HA-W transformation of the HA-ZrO_2 composites look the same as the HA-Al_2O_3 composites. The transformation temperature is 1100 °C (Figs. 6 – 7) and HA was transformed to W completely as previous. At 1207 °C, ZrO_2 (Fig. 6) changed from a monoclinic to tetragonal structure. At the same temperature, calcium ions coming from HA diffused into the zirconia phase and formed the calcium zirconate phase (CZ) ($CaZrO_3$). In addition, slag formation occurred between 1000 – 1300 °C and the addition of CIG is the key to slag formation (Fig. 6). DTA analysis indicated that the endotherm was observed between 1150 – 1250 °C as a consequence of the crystal formation of $CaZrO_3$ and phase transformation of ZrO_2 according to Eq. 2 – 3 as predicted thermodynamically (Fig. 7).

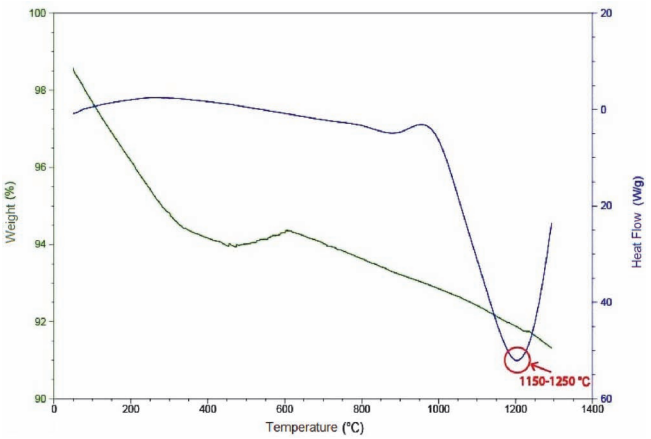

Fig. 6: The DTA analysis result of the HZC5 composite.

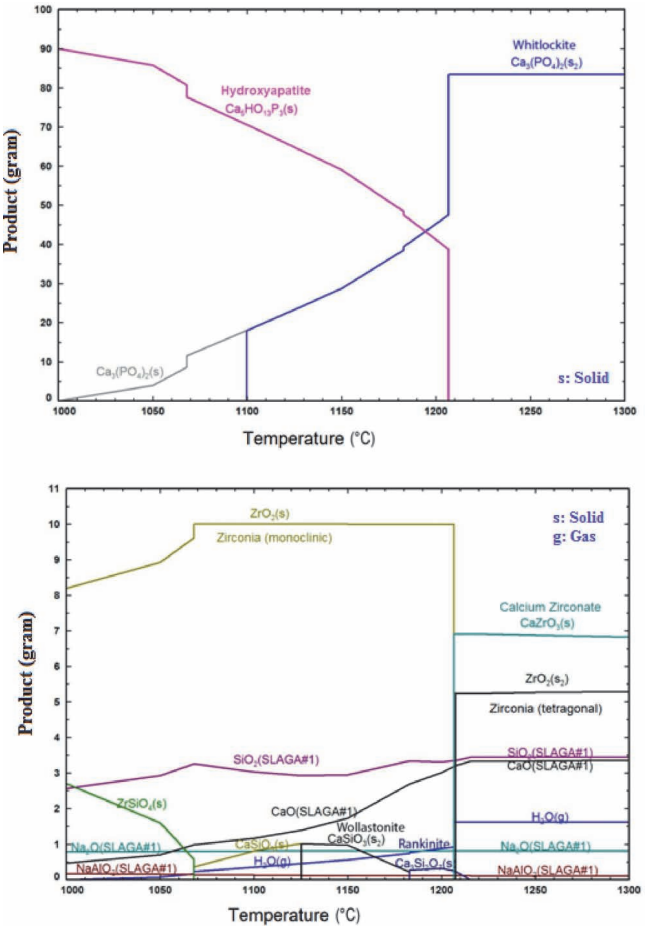

Fig. 7: The FactSage equilibrium diagram of the HZC5 composite.

$$ZrO_2\ (\text{Monoclinic}) \rightarrow ZrO_2\ (\text{Tetragonal}) \quad (2)$$

$$ZrO_2 + CaO \rightarrow CaZrO_3 \quad (3)$$

The results of HZC10 are slightly different. There was no depletion of ZrO_2 and no formation of $CaZrO_3$. The slag was the dominant phase based on the higher amount of CIG addition, which possibly lowered the melting tem-

perature by forming eutectics. The endothermic phase transformation of ZrO_2 occurred nearly at 1170 °C, lower than 5 wt% CIG added composites most probably due to missing $CaZrO_3$ phase formation (Fig. 9). The decomposition of HA also occurred faster than HZC5 possibly because of the higher amount of slag present in the system.

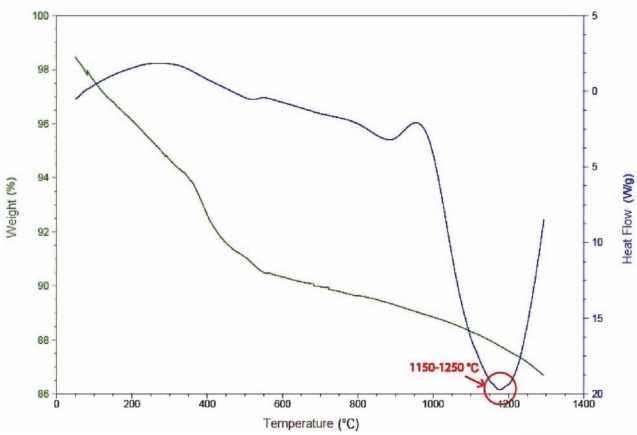

Fig. 8: The DTA analysis result of the HZC10 composite.

(3) XRD Analysis

Fig. 10 and Fig. 11 depict XRD patterns and corresponding phases obtained for HA-Al_2O_3 and HA-ZrO_2 composites sintered at 1000 °C and 1300 °C. The product phases of HA-Al_2O_3-CIG composites after sintering at 1000 °C are HA, Al_2O_3 and W whereas composites sintered at 1300 °C include HA, Al_2O_3, W and $Ca_2Al_2SiO_7$ and sodium calcium silicate (SCS) for 10 wt% CIG in addition. Conversely, for composites HA-ZrO_2 with 5 and 10 wt% CIG addition after sintering at 1000 °C, phases formed are HA, ZrO_2, W, calcium zirconate (CZ) whereas HZC5 composite sintered at 1300 °C included HA, ZrO_2, W, SCS. Also, HZC10 composite sintered at 1300 °C contained calcium silicate (CS) phase in addition to these phases.

(4) SEM-EDS analysis

Figs. 12a – 12f present the microstructure and corresponding EDS results of HAC5 and HAC10 sintered at 1000 °C and 1300 °C. When Fig. 12a is compared with Fig. 12c, grain growth is evident, and this occurred because of increasing sintering temperature. When Fig. 12a is compared with Fig. 12b, the porosity decreased and a more compact microstructure was obtained with increasing CIG content.

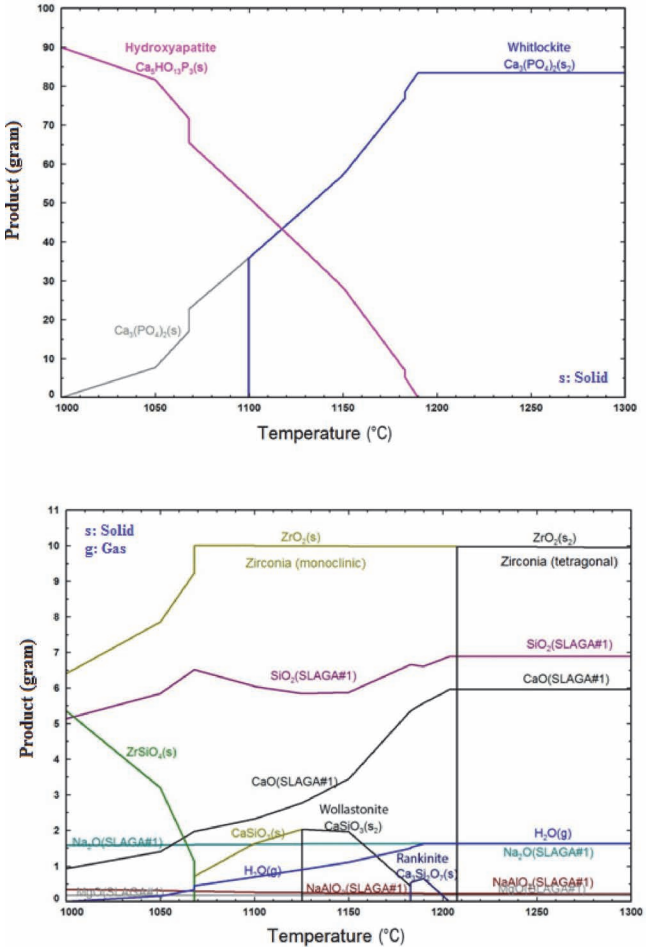

Fig. 9: The FactSage equilibrium diagram of the HZC10 composite.

Fig. 13a – 13g present the microstructure and corresponding EDS results of HZC5 and HZC10 sintered at 1000 – 1300 °C. When Fig. 13a – b is compared with Fig. 13c-d, grain growth occurred with increasing sintering temperature. Increase of CIG content also enhanced grain growth as clearly seen in Fig. 13(a) – 13(b) and Fig. 13(c) – 13(d). Crack formation was observed in HZC10 which occurred as a result of glassy phase formation after solidification (Fig. 14).

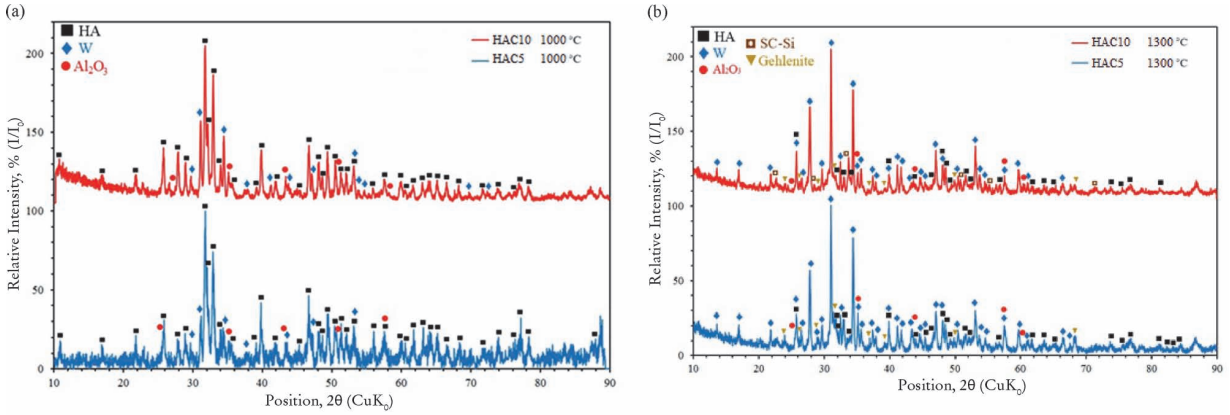

Fig. 10: XRD diagrams of HAC5 and HAC10 (a) sintered at 1000 °C (b) sintered at 1300 °C.

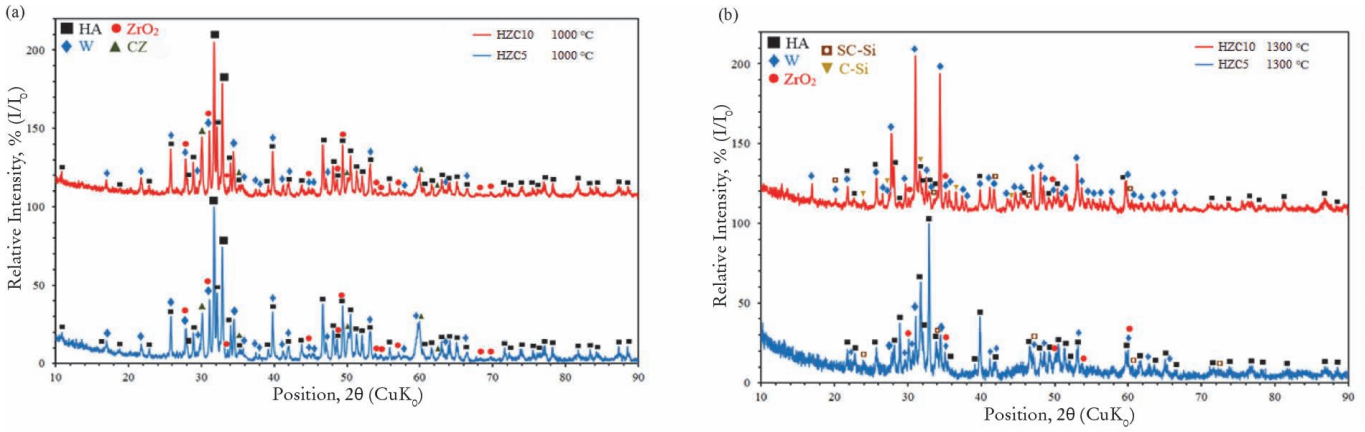

Fig. 11: XRD diagrams of HZC5 and HZC10 (a) sintered at 1000 °C (b) sintered at 1300 °C.

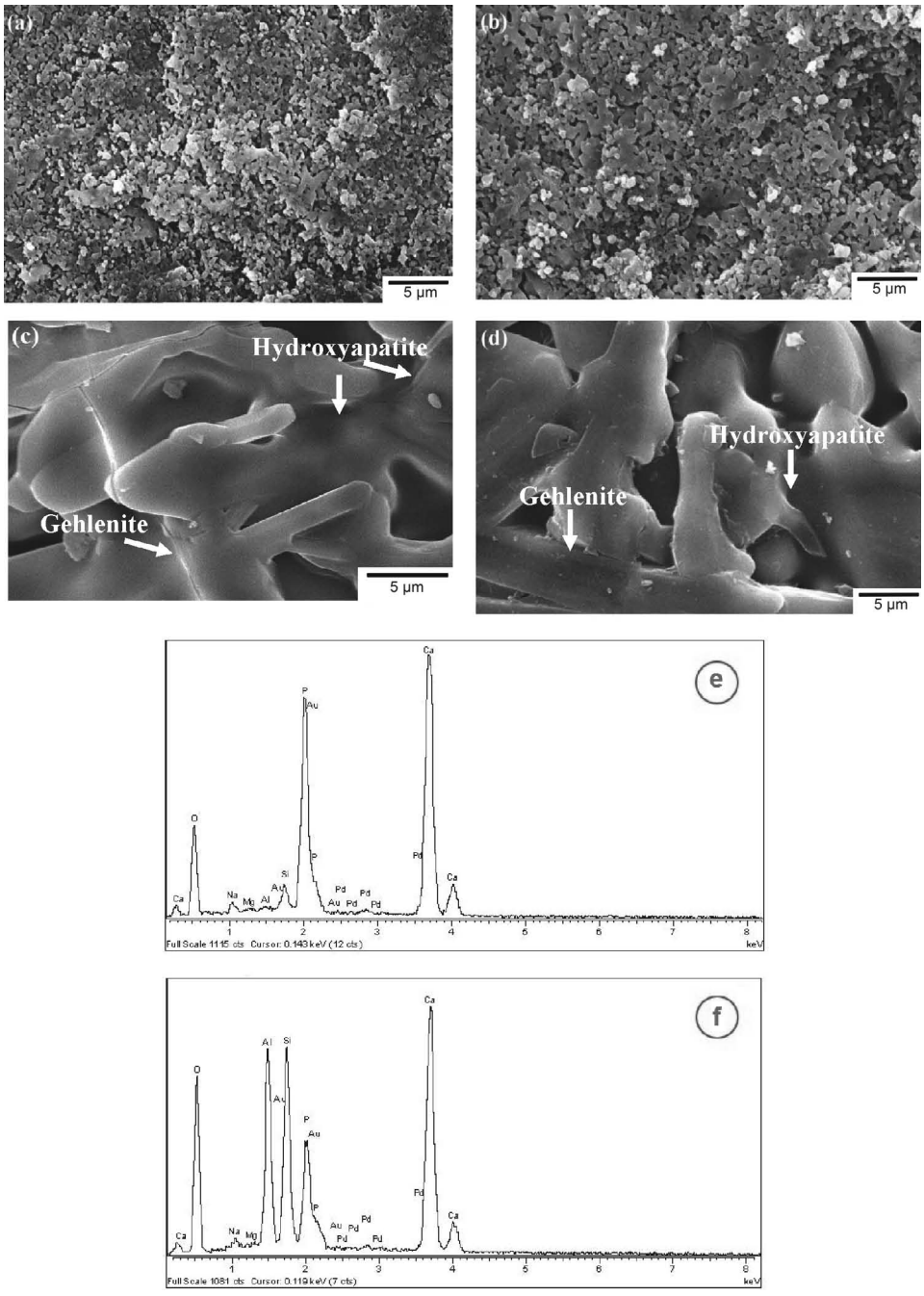

Fig. 12: Microstructures and EDS analysis of HA-Al_2O_3 composites (a) HAC5 at 1000 °C, (b) HAC10 at 1000 °C, (c) HAC5 at 1300 °C, (d) HAC10 at 1300 °C, (e) EDS analysis results of hydroxyapatite phase, (f) EDS analysis results of gehlenite phase.

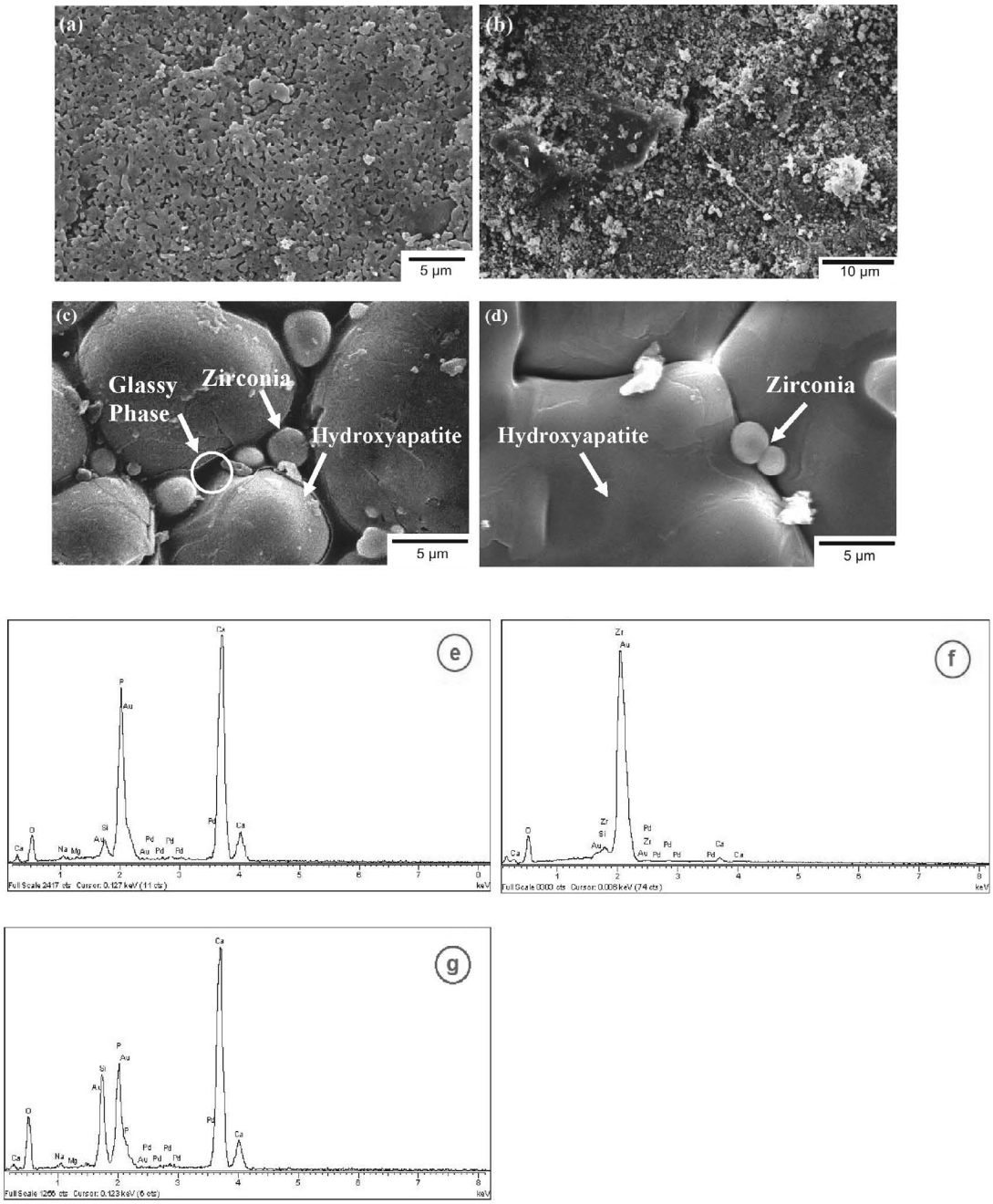

Fig. 13: Microstructures and EDS analysis of HA-ZrO_2 composites (a) HZC5 at 1000 °C, (b) HZC10 at 1000 °C, (c) HZC5 at 1300 °C, (d) HZC10 at 1300 °C, (e) EDS analysis of hydroxyapatite phase, (f) EDS analysis of zirconia phase (g) EDS analysis of glassy phase.

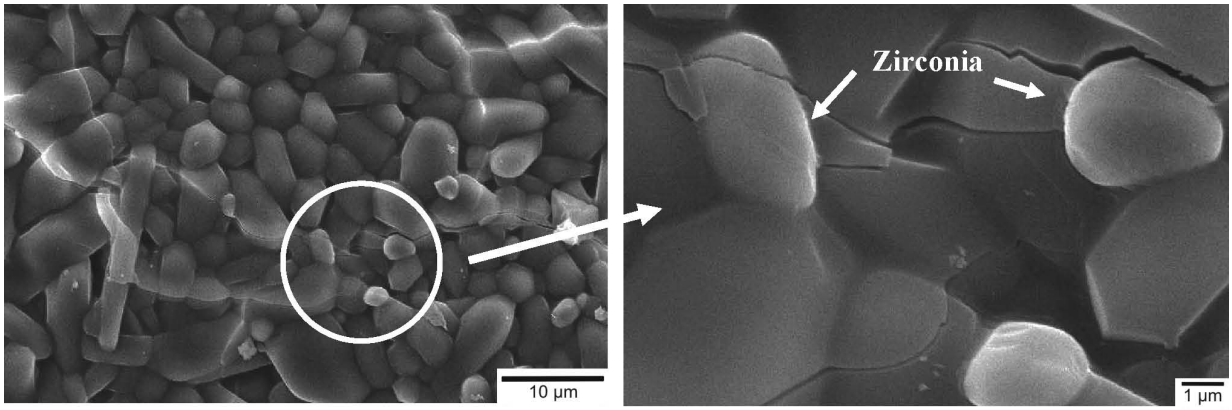

Fig. 14: The crack formation of HZC10 sintered at 1300 °C.

(5) Mechanical test results

Fig. 15 summarizes the compression strength and Vickers microhardness results of samples sintered at different temperatures. Mechanical properties of HAC composites increased with increasing CIG content. In the HAC10 composite, glassy phase (SCS) formed above 1200 °C, which caused an increase in hardness and strength values (129.36 HV; 53.82 MPa). For the HZC composites, the highest Vickers microhardness was obtained in HZC5 sintered at 1300 °C. The highest compression strength was measured again in HZC5 sintered at 1200 °C. For HZC composites, when sintering temperature increased, calcium ions diffusing from HA into the zirconia phase formed a calcium zirconate phase. Addition of excess CIG (glass powders) enhanced the HA decomposition to TCP (tricalcium phosphate), possibly the result of liquid slag formation as noticed in Fig. 6. Additionally, there has been a phase change from monoclinic to tetragonal zirconia at 1300 °C bringing a volume increase as expected and SCS occurred at this temperature. A dramatic reduction in the mechanical properties of the HZC10 composite (16.42 MPa; 39.66 HV) was observed because of the formation of CS glassy phase (Fig. 13). When HZC composites were compared with HAC composites, the microstructures and mechanical properties of the former were shown to be superior.

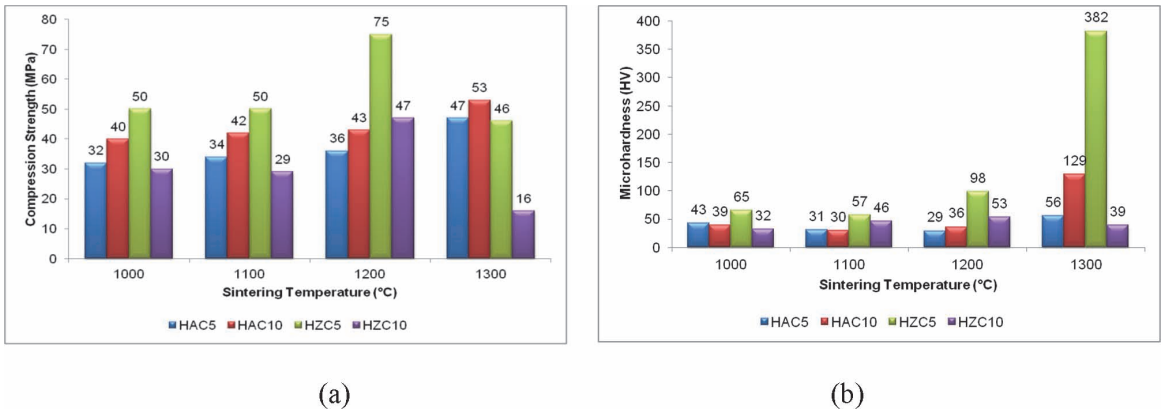

Fig. 15: Mechanical properties of HAC-HZC composites (a) Compression strength (b) Microhardness.

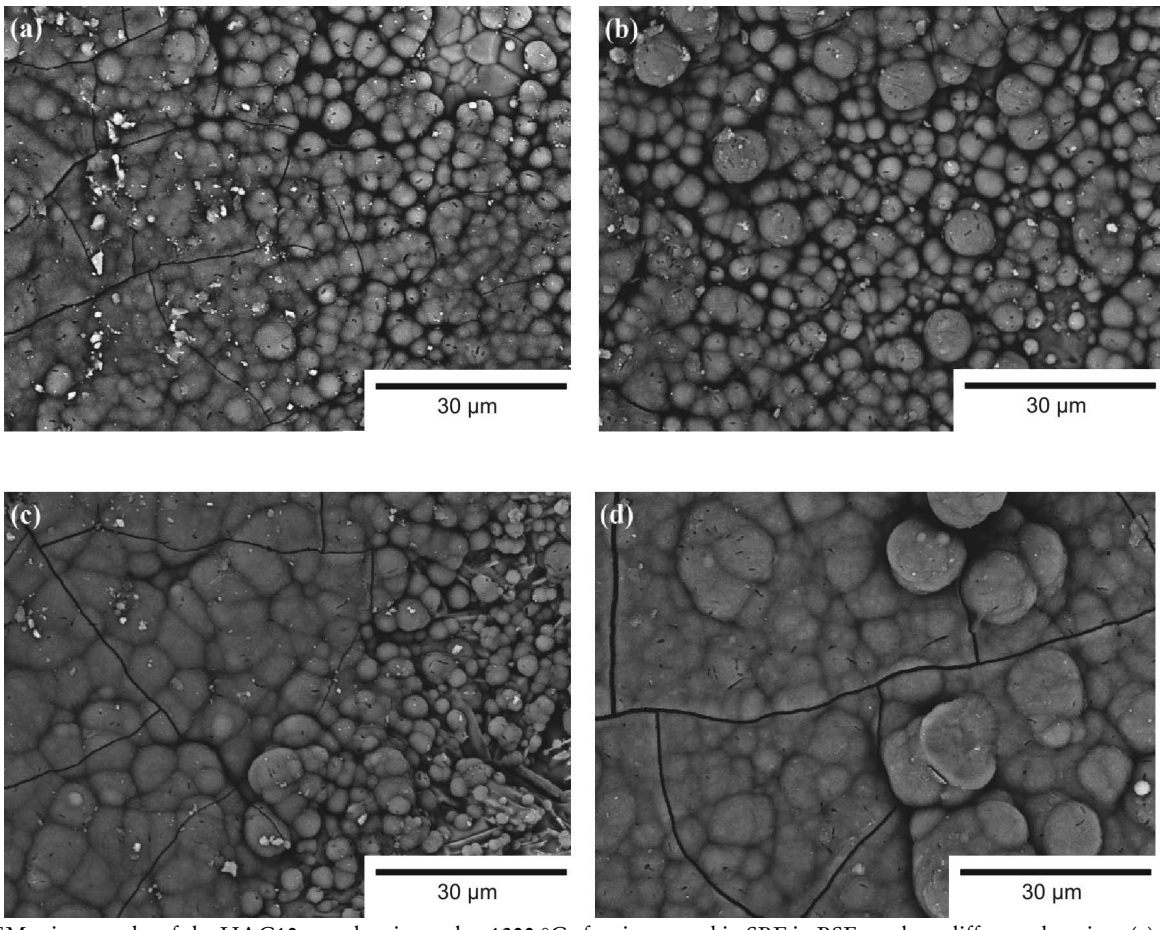

Fig. 16: SEM micrographs of the HAC10 samples sintered at 1200 °C after immersed in SBF in BSE mode at different duration; (a) 1, (b) 2, (c) 3, (d) 4 weeks.

(6) Biocompatibility test results

The *in vitro* bioactivity tests were performed on the composites exhibiting highest physical and mechanical properties. Fig. 16, Fig. 17, and Fig. 18 show, respectively, surface morphology of HAC10, HZC5 composite sintered at 1200 °C, and HZC5 composite sintered at 1300 °C after 1, 2, 3 and 4 weeks of immersion in SBF.

Starting from the first week, intensive apatite layer formation for all samples was determined. When the immersion time in SBF was increased, the size and quantity of the apatite layer increased, too, as expected. Surprisingly, the size and quantity of the apatite layer also increased with increasing sintering temperature. This is probably based on an excessively smooth morphology, well-arranged grains, and presence of the glassy phase enhancing apatite formation at higher sintering temperatures. At the end of 4 weeks, the samples' surfaces were totally covered by the apatite layer. For the HZC5 composites sintered at 1200 °C, the existing apatite nucleation was observed only around ZrO_2 grains in the first week. At the end of 3 weeks, the apatite accumulation also occurred on the ZrO_2 grains. For HZC5 composites sintered at 1300 °C, the apatite nucleation was more abundant than the other two composites and ZrO_2 grains were covered by the apatite layer starting from the first week. Of all the composites, the HZC5 sintered at 1300 °C showed the fastest apatite formation. Following the bioactivity tests, the samples were dried for characterization of the apatite layer formed during bioactivity tests. Many cracks were observed on the apatite layer after drying caused by thermal shock during rapid cooling process (Figs. 16, 17, and 18).

Fig. 19 illustrates the ALP activity of the HZC5 composite sintered at 1200 °C after 14 days of culture, whereas Fig. 20 shows the Alizarin Red S Staining after 7 days of culture. The growing bones need alkaline phosphates. Therefore, alkaline phosphate production is an indicator of biological activity. The sample displayed significantly higher levels of ALP secretion.

Fig. 21 shows the cell number of the HZC5 composite sintered at 1200 °C after the experiment. The cell number increased in a time-dependent manner. Positive cell production was initially detected at Day 7 and then followed by significant upregulation at Day 14.

Cell viability of the HZC5 composite sintered at 1200 °C was > 95 % for all. When the biocompatibility test results (*in vitro* and *in vivo*) were evaluated, it was concluded that samples were definitely biocompatible.

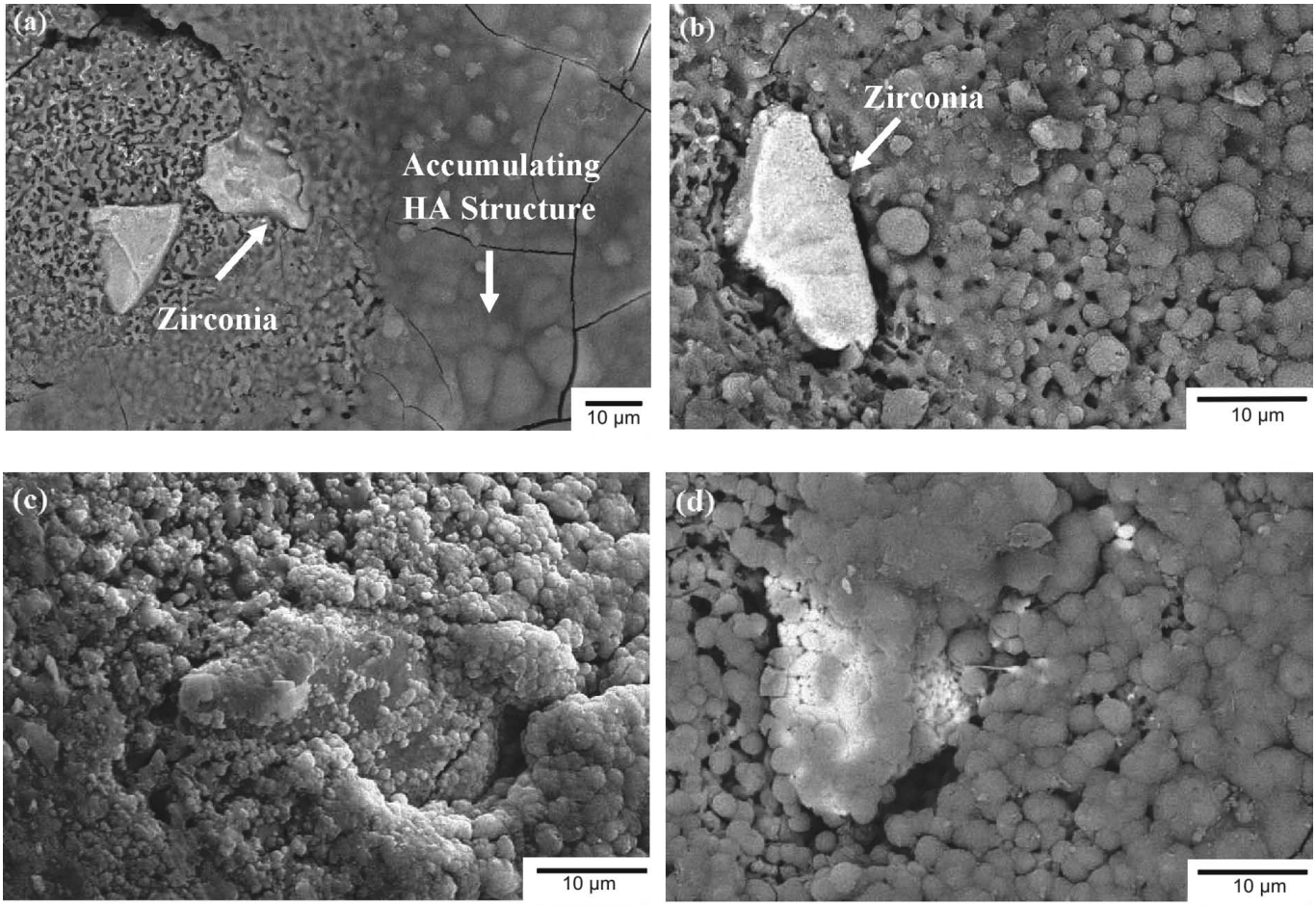

Fig. 17: SEM micrographs of the HZC5 samples sintered at 1200 °C after immersed in SBF in BSE mode at different duration; (a) 1, (b) 2, (c) 3, (d) 4 weeks.

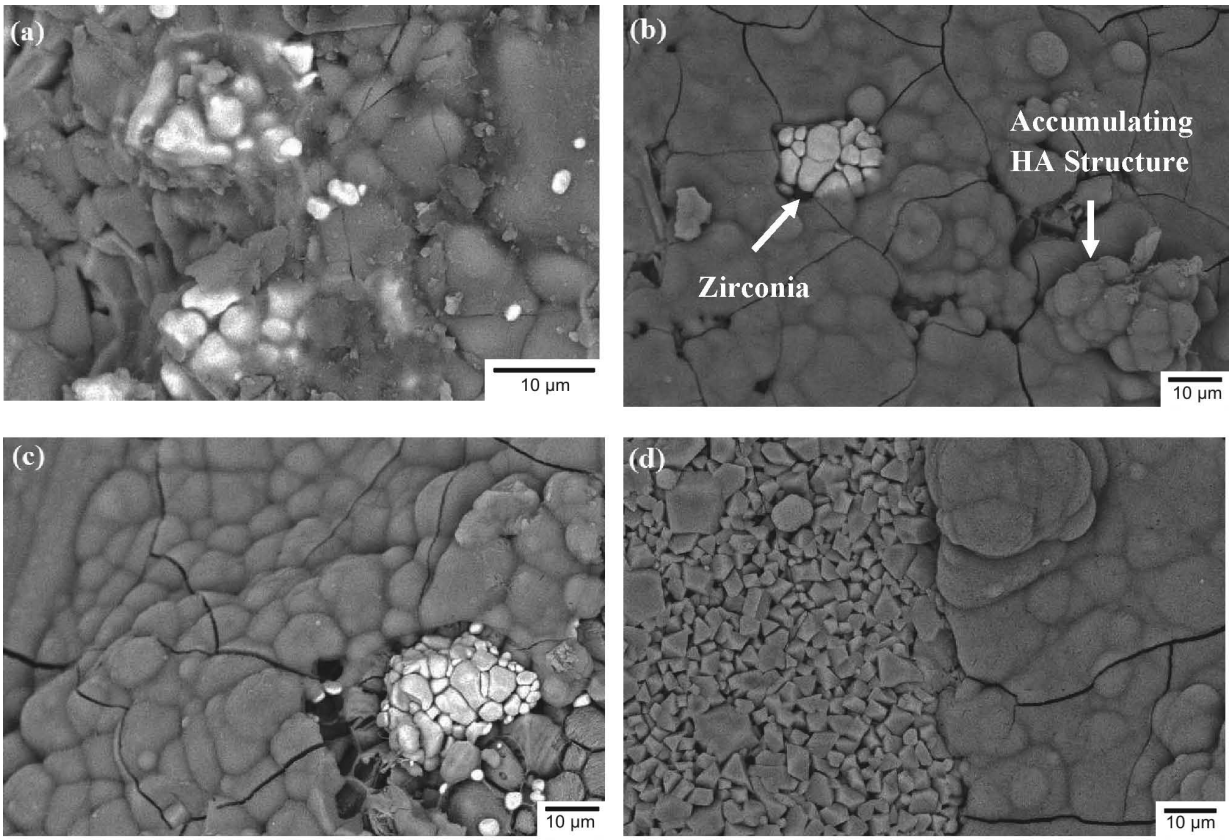

Fig. 18: SEM micrographs of the HZC5 samples sintered at 1300 °C after immersed in SBF in BSE mode at different duration; (a) 1, (b) 2, (c) 3, (d) 4 weeks.

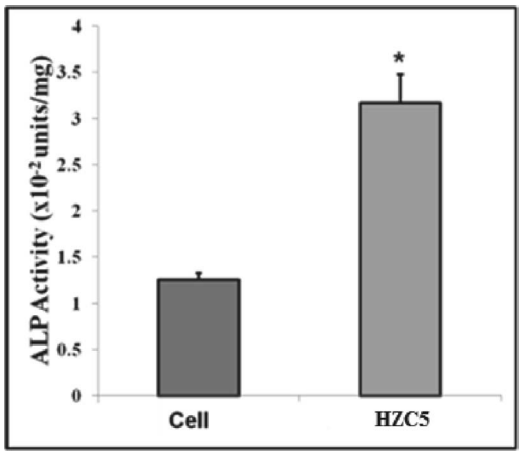

Fig. 19: The ALP activity of HZC5 composite sintered at 1200 °C after 14 days of culture.

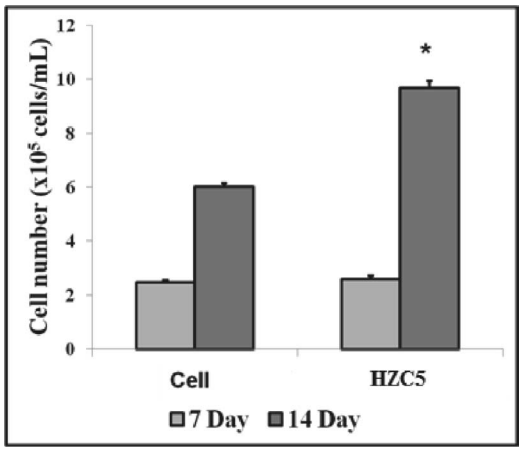

Fig. 21: The cell number of the HZC5 composite sintered at 1200 °C after 7 and 14 days of culture.

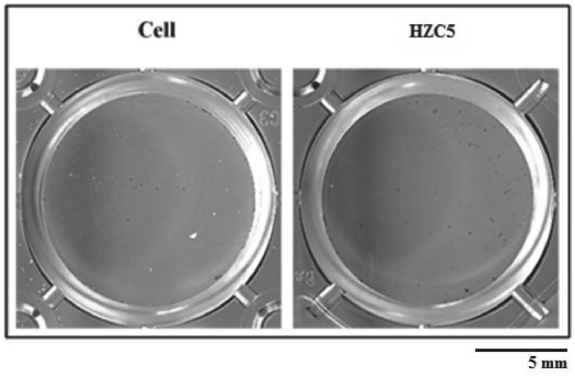

Fig. 20: The determination of osteoblast differentiation of HZC5 composite by Alizarin Red Staining after 7 days of culture.

IV. Conclusions

The findings of this study are summarized as follows:

1. The highest density, the lowest porosity, the highest Vickers microhardness, and the highest compression strength values were obtained in HAC10 composites sintered at 1300 °C among HA-Al_2O_3 composites. The compression strength and microhardness of composites increased with increasing CIG content.
2. The highest density and hardness values were measured in the HZC5 composite at 1300 °C, while the highest compression strength was obtained with HZC5 composites at 1200 °C among all examined

composites. The compression strength and the microhardness of the composites decreased with increasing CIG content.

3. Sintering temperature played an important role in phase distribution, just as expected. With increasing sintering temperature, tricalcium phosphate (TCP), whitlockite (W) and glassy phases were formed from the decomposition of hydroxyapatite.
4. Grain growth occurred with increasing sintering temperature as expected for all composites. When the microstructural properties of HA-Al_2O_3 and HA-ZrO_2 composites were compared, the HA-Al_2O_3 composite's porosity was decreased and the microstructure became denser with increasing CIG content. For HA-ZrO_2 composites, increased CIG content enhanced grain growth, and glassy phases were formed contributing to crack formation during cooling.
5. The composites having the best physical and mechanical properties also showed improved bioactive properties. Starting from the first week, intensive apatite layer formation on the surface was determined. Apatite nucleation was also observed on ZrO_2 grains. At the end of the four weeks, the matrix was completely coated with an apatite layer.
6. The ALP activity level and cell number of the samples increased after 7 and 14 days of culture.
7. Optimum CIG content was provided based on the increase in the mechanical properties and bioactivities of the composites. The microstructure, mechanical properties and bioactivities of the HA-Al_2O_3 composites were found to be lower than those of the HA-ZrO_2 composites. Of all the test results, the optimum microstructure, mechanical properties and biocompatibilities were obtained for the HZC5 composite sintered at 1200 °C.
8. These results can be considered an indication for the potential use of these ternary composites for bone repair and/or bone replacements in orthopedics.

Acknowledgments

This research was supported by TUBITAK under project code 213M633.

We are grateful to Prof. Dr Faik Nuzhet Oktar, Dr Joshua Chou and Research Assistant Onur Tazegul.

References

1 Engin, N.O., Tas, A.C.: Manufacture of macroporous calcium hydroxyapatite bioceramics, *J. Eur. Ceram. Soc.*, **19**, 2569 – 2572, (1999). Doi:10.1016/S0955 – 2219(99)00131 – 4

2 Kwon, S.H., Jun, Y.K., Hong, S.H., Kim, H.E.: Synthesis and dissolution behavior of β-TCP and HA/β-TCP composite powders, *J. Eur. Ceram. Soc.*, **23**, 1039 – 1045, (2003). Doi:10.1016/S0955 – 2219(02)00263 – 7

3 Rabiee, S.M., Moztarzadeh, F., Solati-Hashjin, M.: Synthesis and characterization of hydroxyapatite cement, *J. Mol. Struct.*,**969**,: 172 175, (2010). Doi:10.1016/j.molstruc.2010.01.068

4 Hannora, A.E.: Preparation and characterization of Hydroxyapatite/Alumina nanocomposites by high-energy vibratory ball milling, *J. Ceram. Sci. Tech.*, **5**, 293 298, (2014). Doi: 10.4416/JCST2014 – 00019

5 Descampsa, M, Boilet, L, Moreaua, G., Tricoteaux, A., Lud, J., Leriche, A., Lardot, V., Cambier, F.: Processing and properties of biphasic calcium phosphates bioceramics obtained by pressureless sintering and hot isostatic pressing, *J. Eur. Ceram. Soc.,***33**, 1263 1270, (2013). Doi:10.1016/j.jeurceramsoc.2012.12.020

6 Brown, O., McAfee, M., Clarke, S., Buchanan, F.: Sintering of biphasic calcium phosphates, *J. Mater. Sci. – Mater. M.* **21**, 2271 – 2279, (2010). Doi: 10.1007/s10856 – 010 – 4032 – 6

7 Kim, S.J., Bang, H.G., Song, J.H., Park, S.Y.: Effect of fluoride additive on the mechanical properties of Hydroxyapatite/Alumina composites, *Ceram. Int.*, **35**, 1647 – 1650, (2009). Doi:10.1016/j.ceramint.2008.07.016

8 Goller, G., Demirkiran, H, Oktar, F.N., Demirkesen, E.: Processing and characterization of bioglass reinforced hydroxyapatite composites,*Ceram. Int.*, **29**, 721 – 724, (2003). Doi:10.1016/S0272 – 8842(02)00223 – 7

9 Demirkol, N., Oktar, F.N., Kayali, E.S.: Influence of niobium oxide on the mechanical properties of hydroxyapatite, *Key Eng. Mat.*, 529 – 530, 29 – 33, (2013). Doi:10.4028/www.scientific.net/KEM.529 – 530.29

10 Rao, R.R., Kannan, T.S.: Synthesis and sintering of hydroxyapatite-zirconia composites, *Mater. Sci. Eng.* **20**, 187 – 193 (2002) Doi:10.1016/S0928 – 4931(02)00031 – 0

11 Mobasherpour, I., Hashjin, M.S., Toosi, S.S.R., Kamachali, R.D.: Effect of the addition ZrO_2-Al_2O_3 on nanocrystalline hydroxyapatite bending strength and fracture toughness, *Ceram. Int.* **35**; 1569 – 1574 (2009). Doi:10.1016/j.ceramint.2008.08.017

12 Ayed; F:B:, Bouaziz; J.: Sintering of tricalcium phosphate-fluorapatite composites by addition of alumina, *Ceram. Int.*, **34**, 1885 – 1892, (2008). Doi:10.1016/j.ceramint.2007.07.017

13 Samodurovaa, A., Kocjana, A., Swainb, M.V., Kosmaca, T.: The combined effect of alumina and silica co-doping on the ageing resistance of 3Y-TZP bioceramics, *Acta Biomater.*; **11**, 477 – 487, (2015). Doi:10.1016/j.actbio.2014.09.009

14 Hisbergues, M., Vendeville, S., Vendeville, P.: Zirconia: established facts and perspective for a biomaterial in dental, *J. Biomed. Mater. Res. B.*, **88**, 519 – 529, (2009). Doi: 10.1002/jbm.b.31147

15 Daou, E.E.: The zirconia Ceramic: Strengths and weaknesses, *Open Dent. J.*, **8**, 33 – 42, (2014). Doi: 10.2174/1874210601408010033

16 Evis, Z.: Reactions in hydroxylapatite-zirconia composites, *Ceram. Int.* **33**, 987 – 991, (2007). Doi:10.1016/j.ceramint.2006.02.012

17 Faure, J., Drevet, R., Lemelle, A., Ben Jaber, N., Tara, A., El Btaouri, H., Benhayoune, H.: A new sol-gel synthesis of 45S5 bioactive glass using an organic acid as catalyst, *Mater. Sci. Eng.*, **47**, 407 – 412, (2015). Doi:10.1016/j.msec.2014.11.045

18 Verne, E., Ferraris, S., Cassinelli, C., Boccaccini, A.R.: Surface functionalization of bioglass with alkaline phosphatase, *Surf. Coat. Tech.*, **264**, 132 – 139, (2015). Doi:10.1016/j.surfcoat.2015.01.001

19 Chen, Q.Z., Thouas, G.A.: Fabrication and characterization of sol-gel derived 45S5 Bioglass®-ceramic scaffolds, *Acta Biomater.*, **7**, 3616 – 3626, (2011). Doi:10.1016/j.actbio.2011.06.005

20 Yelten, A., Yilmaz, S., Oktar, F.N.: Comparison of microstructures of bovine hydroxyapatite and sol-gel derived porous alumina-hydroxyapatite biocomposite powders, *Key Eng. Mater.*, **493 – 494**, 551 – 555, (2012). Doi: 10.4028/www.scientific.net/KEM.493 – 494.551

21 Pujiyanto, E., Tontowi, A.E., Wildan, M.W., Siswomihardjo, W.: Porous hydroxyapatite-zirconia composites prepared by powder deposition and pressureless sintering, *Adv. Mater. Res.*, ; **445**, 463 – 468, (2012). Doi: 10.4028/www.scientific.net/AMR.445.463

22 Salman, S., Oktar, F.N., Gunduz, O., Agathopoulos, S., Ovecoglu, M.L., Kayali, E.S.: Sintering effect on mechanical properties of composites made of bovine hydroxyapatite

(BHA) and commercial inert glass (CIG), *Key Eng. Mater.*, **330 – 332**, 189 – 192, (2007).
Doi: 10.4028/www.scientific.net/KEM.330 – 332.189

[23] Demirkol. N., Oktar, F.N., Kayali, E.S.: Influence of commercial inert glass addition on the mechanical properties of commercial synthetic hydroxyapatite, *Acta Phys. Pol. A.*, **123**, 427 – 429, (2013). Doi: 10.12693/APhysPolA.123.427

[24] Pelton, A.D., Thompson, W.T., Bale, C.W., Eriksson, G.: FACT thermochemical database for calculations in materials chemistry at high temperatures, *Materials Chemistry at High Temperatures* **1**, 231 – 250, (1990).
Doi: 10.1007/978 – 1-4612 – 0481 – 7_18

[25] Kokubo, T., Takadama, H.: How useful is SBF in predicting *in vivo* bone bioactivity?. *Biomaterials*, **27**, 2907 – 2915, (2006).
Doi:10.1016/j.biomaterials.2006.01.017

[26] Kokubo, T.: Bioactive glass Ceramics: properties and applications, *Biomaterials*, **12**, 155 – 163 (1990).
Doi:10.1016/0142 – 9612(91)90194-F

[27] Maniatopoulos, C., Sodek, J., Melcher, A.H.: Bone formation *In Vitro* by stromal cells obtained from bone marrow of young adult rat, *Cell Tissue Res.*, **254**, 317 – 330, (1988).
Doi:10.1007/BF00225804